

MICROWAVE MEASUREMENTS  
OF PROJECTILE KINEMATICS  
WITHIN LAUNCHER BARRELS

By

R. E. Hendrix

von Kármán Gas Dynamics Facility

ARO, Inc.

a subsidiary of Sverdrup and Parcel, Inc.

November 1962

ARO Project No. 386080

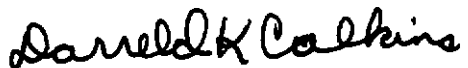
# *Contrails*

**ABSTRACT**

Microwave reflectometry has been applied successfully to the study of the kinematic behavior of projectiles within launcher barrels and pistons within compression (pump) tubes in the Hypervelocity Pilot Range of the von Kármán Gas Dynamics Facility. Well-defined mathematical treatment enables the calculation of an accurate time history of projectile position inside its launcher barrel. Microwave excitation in extraneous modes has been attenuated, resulting in an increase in the accuracy of the reflectometer system.

**PUBLICATION REVIEW**

This report has been reviewed and publication is approved.



Darreld K. Calkins  
Major, USAF  
AF Representative, VKF  
DCS/Test



Jean A. Jack  
Colonel, USAF  
DCS/Test

# *Contrails*

CONTENTS

	<u>Page</u>
ABSTRACT . . . . .	iii
NOMENCLATURE . . . . .	vii
1.0 INTRODUCTION . . . . .	1
2.0 DESCRIPTION OF THE REFLECTOMETER APPARATUS . . . . .	1
3.0 THEORY OF OPERATION . . . . .	2
4.0 REFLECTOMETER RESULTS . . . . .	5
5.0 TREATMENT OF DATA . . . . .	5
6.0 DIGITAL READOUT SYSTEM . . . . .	7
7.0 CONCLUSIONS . . . . .	9
REFERENCES . . . . .	9
APPENDIX I: Waveguide Modes . . . . .	11

ILLUSTRATIONS

Figure

1. Microwave Reflectometer Apparatus . . . . .	13
2. Microwave Reflectometer with 20-mm Barrel . . . . .	14
3. Microwave Reflectometer with 40-mm Barrel . . . . .	15
4. Cutoff Wavelengths for Circular Guides . . . . .	16
5. Waveguide Wavelength versus Oscillator Frequency for Prevalent Modes in 20-mm and 40-mm Barrels . . . . .	17
6. Oscillogram: 20-mm Compression Tube Reflectom- eter Signal. . . . .	18
7. 20-mm Compression Tube Piston Displacement versus Time . . . . .	19
8. Oscillogram: Medium Velocity, 40-mm Cold-Gas Gun Shot No. 401 . . . . .	20
9. Oscillogram: High Velocity, 40-mm Cold-Gas Gun Shot No. 466 . . . . .	21
10. 40-mm Projectile Displacement versus Time, Shot No. 401 . . . . .	22

<u>Figure</u>	<u>Page</u>
11. 40-mm Projectile Displacement versus Time, Shot No. 466. . . . .	23
12. Analog-to-Digital Reflectometer Readout System . . . . .	24
13. Digital System Waveforms . . . . .	25
14. Oscillogram: Digital System Operation. . . . .	26
15. Four of the Simple Modes of Waves in a Circular Waveguide. . . . .	27
16. Attenuation versus frequency for a Hollow Copper Barrel with $b = 20$ mm . . . . .	28
17. Plot Showing the Bessel Functions of the First Kind, $J_0(r_n)$ and $J_1(r_n)$ . . . . .	29

## NOMENCLATURE

a	Instantaneous peak acceleration, ft/sec <sup>2</sup>
b	Circular waveguide radius, cm
f	Accelerating force, poundals
J <sub>0</sub>	Bessel function of the first kind of order zero
J <sub>0</sub> '	First derivative of Bessel function of the first kind of order zero
J <sub>1</sub>	Bessel function of the first kind of first order
J <sub>1</sub> '	First derivative of Bessel function of the first kind of first order
k <sub>1</sub>	Constant term, ft/sec
k <sub>2</sub>	Constant term, ft
k <sub>3</sub>	Constant term, 1/sec
m	Mass, lb
r <sub>n</sub>	Bessel function zero solution
t	Time, sec
V <sub>a</sub>	Average projectile velocity, ft/sec
x	Distance travelled by projectile, ft
e	Naperian base, 2.718
λ	Wavelength, cm
λ <sub>c</sub>	Wavelength corresponding to cutoff frequency, cm
λ <sub>g</sub>	Wavelength within the waveguide, cm
λ <sub>0</sub>	Wavelength in free space, cm

# *Contracts*



## 1.0 INTRODUCTION

The kinematic behavior of projectiles in launcher barrels and of free pistons in pump tubes is of great interest in the development of hypervelocity range launchers and radio telemeters. An assortment of instrumentation systems has been used by various investigators in attempts to obtain data describing projectile kinematics. Crusher switches, installed at stations along the length of launcher barrels, have been used to announce arrival of the projectile at a few discrete positions. The use of similarly distributed pressure transducers has been tried. Attempts have also been made to infer projectile dynamics from barrel strain measurements. Shortcomings are evident in each of these schemes. Crusher switches require modification of the barrel; they usually have low reliability, absorb energy from the projectile, and introduce the risk of damage to the round. Pressure measurements also require barrel modification, and they limit kinematic data to the few stations at which transducers have been installed; the additional inconvenience of time lag in transducer response arises. Little needs to be said of the complications in dynamic loading of structures which must be considered if barrel strain measurements are used as a means of determining projectile velocities and accelerations during launching.

There is remarkable similarity between the ordinary launcher barrel with its projectile and the classical, cylindrical waveguide with a moveable shorting stub. This similarity suggests microwave reflectometry as an attractive means to measurement of projectile kinematics. Barrel modification is limited to the installation of a single, simple antenna. Projectile position data are continuous, rather than being limited to announcement at discrete barrel stations. Frequency response of microwave apparatus is more than sufficient to accommodate the range of velocities encountered. Such a microwave reflectometer was used by Pennelegion (Ref. 1) as early as 1958 but has not been extensively employed since. Early attempts at projectile kinematic studies through microwave techniques within the von Kármán Gas Dynamics Facility (VKF), Arnold Engineering Development Center (AEDC), Air Force Systems Command (AFSC), U. S. Air Force, have resulted in the work described here.

## 2.0 DESCRIPTION OF THE REFLECTOMETER APPARATUS

A photograph of the microwave reflectometry system used in VKF in projectile kinematic measurements in launcher barrels and pump tubes is given in Fig. 1, and schematics of the system are shown in Figs. 2 and 3.

---

Manuscript released by author October 1962.

A directional coupler (Hewlett-Packard X752C) is inserted between an X-band klystron (Varian Associates X-13) and a probe antenna to supply microwave energy to the barrel through flexible cable (RG-9/AU).

The microwave signal appearing at the output of the auxiliary guide in the directional coupler is detected by a modified 1N26 crystal detector and matched load (Polytechnic Research and Development Co. No. 601). The detected signal is amplified by 20 db through an amplifier (Hewlett-Packard model 450A) and filtered through "parallel T" 60-cps and 120-cps rejection filters before magnetic tape recording.

### 3.0 THEORY OF OPERATION

An experimental 20-mm compression tube and 40-mm cold-gas gun barrel have been used as circular waveguides in the VKF microwave reflectometry system for producing projectile kinematic data.

The klystron excites the barrel as a circular waveguide in one distinguishable mode through a probe antenna which performs both transmitting and receiving functions. The antenna used in the 40-mm gun barrel is considerably different from the one used in the 20-mm compression tube. Both antennas are described later.

The foreface of the metallic piston or Fiberglas projectile approximates a reflecting termination; i. e., it is analogous to a conventional tuning stub used in making standing wave measurements in waveguides. As sensed by the antenna, the wave reflected from the piston or projectile will undergo cyclic changes in amplitude as the piston traverses the length of the barrel. Reference 2 shows that wavelength inside the guide,  $\lambda_g$ , is a function of the free-space wavelength,  $\lambda_o$ , and the cutoff wavelength,  $\lambda_c$ , and may be expressed as:

$$\lambda_g = \frac{\lambda_o}{\sqrt{1 - \left(\frac{\lambda_o}{\lambda_c}\right)^2}}$$

The cutoff wavelength,  $\lambda_c$ , is a function of the radius,  $b$ , of the waveguide and of a zero solution,  $r_n$ , of an appropriate Bessel function and may be expressed as:

$$\lambda_c = \frac{2\pi b}{r_n}$$

A mathematical analysis of the various modes which may exist in circular waveguides produces the relationship between these modes and the Bessel

function solutions mentioned above. This analysis is given in Appendix I, and a table of cutoff wavelengths for circular guides is provided in Fig. 4, giving  $\lambda_c/b$  for the first several modes.

Although the reflecting surface of the 40-mm projectile used in the cold-gas gun is of Fiberglas, fairly large detected signals (100 millivolts p-p) are obtained because of the relatively high power output of the klystron (200 milliwatts). Still larger detected signals of several hundred millivolts were obtained when the reflectometer was used to study the kinematics of aluminum pistons inside the 20-mm compression tube.

The detected signal is an analog voltage representation of projectile position inside the barrel. It must be assumed that the microwave frequency is constant, that the barrel is excited in only one mode, and that the waveguide wall attenuation is negligible. The analog voltage signal is recorded on magnetic tape; upon its playback into a recording oscillograph, a time history of projectile position within the barrel is recorded. Recording at high tape speed and playback at reduced speed permits magnification of the time axis in the resulting oscillogram. A magnification factor of 32 is customary. The distance travelled by the projectile between successive nodes in the recorded signal is equal to  $\lambda_g/2$ , and time intervals may be read directly from the oscillograph trace.

The antenna used in exciting the 20-mm compression tube consisted of a quarter-wave probe protruding radially into the barrel (Fig. 2). This antenna was sheared by the piston as it left the tube during each firing; however, since the antenna was located near the exit end of the tube, kinematic data were acquired for nearly the entire travel of the piston within the tube.

To excite a particular mode in the 20-mm compression tube, it was necessary that the proper microwave frequency be used. The probe antenna was oriented inside the barrel to coincide with the direction of electric flux, conforming to the pattern of the preferred mode of microwave excitation (Ref. 3). Because the wall of the tube provided the only reasonable location for mounting an antenna connector, a radial, probe antenna was used which provided excitation in a TE mode (see Appendix I). Only the  $TE_{11}$  mode could be propagated in the 20-mm barrel between the frequencies of 8.8 kmc and 11.5 kmc (see Fig. 5). Excitation in this mode and frequency range insured a "clean" recorded signal, free from interference of extraneous modes.

The probe antenna design was altered for use in the reflectometer system with the 40-mm launcher barrel. It was no longer possible to use

a quarter-wave probe protruding into the barrel because of the effect it would have on a telemetry-equipped projectile. Figure 3 shows the antenna arrangement used. The single loop of wire which serves as the antenna does not protrude beyond the inner surface of the barrel wall. Enough energy leaks from this loop to excite the barrel as a circular waveguide. Although the quantity of power radiated from this loop antenna is low as compared with the amount radiated if the loop were extended into the barrel, enough barrel excitation is produced to operate the microwave reflectometer.

Because the plane of the loop antenna is perpendicular to the axis of the barrel, only the transverse electric modes having radial electric field components are excited (Ref. 3). Although only the TE modes are excited (when operating at X-band frequencies), it is impossible to have a single nonevanescant mode, as was the case with the 20-mm pump tube. To operate with a single excited mode above the cutoff frequency in the 40-mm barrel, the frequency range would extend from 4.4 to 5.75 kmc (Fig. 5).

When operating over a limited portion of the X band (8.2 kmc - 9.15 kmc), only the TE<sub>11</sub> and TE<sub>21</sub> modes are energized (see Appendix I). Therefore, if either of these modes could be suppressed, this frequency range could be used with the 40-mm barrel reflectometer without the annoyance of signals from extraneous modes appearing in the data.

It was found that by orienting the loop antenna (made of A. W. G. No. 16 copper wire) to a position approaching perpendicularity with the axis of the barrel, only the TE<sub>21</sub> mode was excited to a detectable degree. The mode in which the barrel was excited was determined by slowly moving a projectile through the barrel and observing the distance travelled by the projectile between successive peaks in the detected output signal.

The main disadvantage resulting from barrel excitation in the TE modes (TE<sub>11</sub> in particular) occurs when the microwave field is propagated in a region of changing pressure and temperature (Ref. 4). The permittivity of the propagating medium will then change according to the temperature and pressure variation. This causes the electric field to rotate and creates amplitude distortion in the reflected wave signal.

The temperature and pressure of the gas ahead of the projectile inside both 20-mm and 40-mm barrels during launchings did not change appreciably. Therefore the reflectometer output from neither barrel was distorted because of a permittivity change. However, if piston kinematic data are to be obtained in a region of changing permittivity, barrel excitation in a radial symmetric mode is preferable. The easiest

of these modes to launch is the  $TM_{01}$ . It may be launched by a simple axial probe antenna.

#### 4.0 REFLECTOMETER RESULTS

Excellent reflected wave data were recorded from aluminum pistons during their travel through the 20-mm compression tube. Figure 6 is an oscillogram of the recorded, reflected wave data obtained during a typical open-end firing of the compression tube. Pressurized air was used to drive a 20-gram aluminum piston through the tube, which was at atmospheric pressure.

The amplitude of the reflected wave signal increases as the piston nears the quarter-wave probe antenna. This increase in amplitude arises from the progressive decrease in attenuation of the microwave signal by the barrel walls as the length of barrel traversed diminishes. A time versus distance plot made from the data obtained from this oscillogram appears in Fig. 7.

The results obtained from the microwave reflectometer when used to instrument the 40-mm barrel have been quite satisfactory. The only major problem encountered occurred during high velocity shots when the detected output signal was somewhat distorted. Figure 8 shows data obtained from a typical, medium velocity firing of the cold-gas gun. Good projectile kinematic information was obtained from these data; treatment of the data appears in a later section.

During several high velocity firings of the cold-gas gun with peak projectile acceleration on the order of 500,000 g, the detected microwave output was distorted. This distortion was apparently caused by mechanical shock to the electronic apparatus or by leakage of the high pressure propellant gas around the projectile and over the antenna. Good data have been obtained from several shots of the cold-gas gun with peak projectile accelerations near 500,000 g by having the projectile fit very snugly into the barrel to prevent leakage of the high pressure gas. The oscillogram shown in Fig. 9 presents the data recorded from such a high-g shot. The distortion appearing in the reflected signal is small and does not hinder the interpretation of the time versus distance information obtained from this trace.

#### 5.0 TREATMENT OF DATA

Data describing projectile kinematics inside the cold-gas gun barrel are useful in determining the launching characteristics of this gun. The

point at which the peak projectile velocity occurs may be located from a time history of the projectile's position within the barrel. The peak acceleration experienced by the projectile during launching may also be derived from these data. The peak acceleration data are especially important in the case of the cold-gas gun because the projectiles fired from this gun are developmental telemetry packages. Performance of these telemeters during flight depends largely upon the ability of the individual telemetry components to withstand high accelerations.

A time versus distance plot was made from the recorded analog microwave signal, and this plot was then curve-fitted to an equation of the form:

$$x = k_1 t + k_2 \left( e^{-k_3 t} - 1 \right)$$

Peak acceleration was then found by twice differentiating this equation with respect to time and setting  $t = 0$ . For example, the time versus distance plot of Fig. 10 was obtained from the recorded data shown in the oscillogram of Fig. 8. Using the boundary condition  $ds/dt = 0$  at  $t = 0$ , the following equation was derived which fitted the data points very closely, as shown by the dotted curve of Fig. 10:

$$x = 2170 t + 0.56 \left( e^{-3880 t} - 1 \right) \text{ ft}$$

The instantaneous velocity is found by:

$$\frac{dx}{dt} = 2170 - 0.56 \left( 3880 e^{-3880 t} - 1 \right) \text{ ft/sec}$$

The instantaneous acceleration is:

$$\frac{d^2x}{dt^2} = 0.56 \left( 3880^2 e^{-3880 t} \right) \text{ ft/sec}^2$$

The peak acceleration thus occurs at  $t = 0$  and is equal to:

$$\frac{d^2x}{dt^2} \text{ (at } t = 0) = 0.56 (3880)^2 = 8.42 \times 10^6 \text{ ft/sec}^2$$

This acceleration,  $8.42 \times 10^6 \text{ ft/sec}^2$ , is equal to approximately 263,000 g.

Peak acceleration is also found by using the  $f = ma$  relationship and computing force from the measured gun chamber pressure and gun bore. The value of peak acceleration found by this method for the launching just described was 243,000 g, which agrees within some eight percent with the results obtained using the reflectometer method.

Other kinematic information such as the peak velocity attained by the projectile inside the barrel is easily obtained from the time versus distance curve. This curve, shown in Fig. 11, represents a time history of the projectile's position inside the barrel during a typical high velocity firing of the cold-gas gun. The velocity,  $V_a$ , may be expressed as:

$$V_{a1} = \frac{\Delta x}{\Delta t} = \frac{0.107 \text{ ft}}{35 \mu\text{sec}} = 3060 \text{ ft/sec}$$

This is the average velocity obtained from the  $x$  vs  $t$  curve with the projectile near the exit end of the barrel. It closely approximates the peak instantaneous velocity in the barrel since the velocity obtained is averaged over a distance of only 0.107 feet.

The average projectile velocity over the last foot of travel inside the barrel is found by:

$$V_{a2} = \frac{\Delta x}{\Delta t} = \frac{0.963 \text{ ft}}{358 \mu\text{sec}} = 2690 \text{ ft/sec}$$

The average velocity from the end of the barrel to a light screen trigger unit located one foot beyond the end of the barrel (Fig. 9) is:

$$V_{a3} = \frac{\Delta x}{\Delta t} = \frac{1 \text{ ft}}{375 \mu\text{sec}} = 2665 \text{ ft/sec}$$

This close correlation between velocity measurements made using the microwave reflectometer and other systems is typical of all the cold-gas gun firings for which an acceptable reflected wave was recorded from the reflectometry system.

## 6.0 DIGITAL READOUT SYSTEM

An analog-to-digital system is used in obtaining a more accurate time versus distance curve. The time intervals between nodes in the recorded signal are read out digitally on electronic counters, whereas previously the time intervals were read directly from the oscillograph trace.

A block diagram of this system appears in Fig. 12. Rectification of the differentiated square-wave pulses appearing at the output of the cathode followers and operation of the electronic counters in the proper triggering mode permits direct digital indication of time intervals corresponding to projectile displacements of half-wavelengths inside the barrel.

The tape-recorded, reflected wave data obtained during a typical firing of the compression tube (Fig. 6) were supplied to the analog-to-digital system simultaneously with playback into the oscillograph. Five

binary stages were used so that division of the recorded frequency was obtained as shown by the waveforms in Fig. 13. Rectification of the differentiated pulses appearing at the various outputs (1A, 1B, 2A, etc.) and operation of all the electronic counters in the negative triggering mode with their respective start and stop gates connected as shown in Fig. 12 gave the results shown in the oscillogram in Fig. 14. This oscillogram shows the time synchronization between the five gating periods of the counters and the recorded reflected-wave signal.

With the system operating as described above, the individual counters should record the following time intervals according to the waveform chart of Fig. 13:

Counter No.	Time Measurement	Piston Displacement
1	interval between first two positive peaks	$\lambda g/2$
2	interval between second and fourth positive peaks	$\lambda g$
3	interval between fourth and eighth positive peaks	$2\lambda g$
4	interval between eighth and sixteenth positive peaks	$4\lambda g$
5	interval between sixteenth and thirty-second positive peaks	$8\lambda g$

The oscillogram (Fig. 14) shows that the counter gating pulses occur exactly as depicted by the above chart with reference to the reflectometer signal. Five digital data points were obtained for 31 half-wavelengths of piston travel inside the compression tube (i. e.,  $1 + 2 + 4 + 8 + 16$  half-wavelengths).

By using additional counters or playing the recorded signal into the analog-to-digital system several times with different gate connections, more digital data points can be obtained. The following chart shows how 14 data points may be obtained for 31 half-wavelengths of piston travel:

Start	Counter Trigger Mode	Stop	Counter Trigger Mode	Time Interval between Positive Peaks of Input Signal
1A	negative	1B	negative	1-2
1A	positive	1B	positive	2-3
2A	negative	2B	negative	2-4



(Chart Continued)

Start	Counter Trigger Mode	Stop	Counter Trigger Mode	Time Interval between Positive Peaks of Input Signal
3B	positive	1B	positive	4-5
3A	negative	2A	negative	4-6
3A	negative	3B	negative	4-8
4A	negative	1A	negative	8-9
4A	negative	2A	negative	8-10
4B	positive	3B	positive	8-12
4A	negative	4B	negative	8-16
5A	negative	2B	positive	16-18
5A	negative	3A	negative	16-20
5B	positive	4B	positive	16-24
5A	negative	5B	negative	16-32

## 7.0 CONCLUSIONS

Microwave reflectometry provides a convenient means to non-interfering, continuous observation of the kinematic behavior of projectiles in launcher barrels and pistons in pump tubes. Velocity measurements obtained by the microwave method fall within one percent of values obtained by other techniques. Values of peak launching acceleration agree within ten percent with data derived by other means. The pulse nature of the microwave reflectometer output signal suits it nicely to digital readout.

## REFERENCES

1. Pennelegion, L. "Instrumentation of the University of Southampton Hypersonic Gun Tunnel." Ph.D Thesis, University of Southampton, England.
2. Terman, Frederick E. Electronic and Radio Engineering. McGraw-Hill Book Company, Inc., New York, 1955. (Fourth Edition).
3. Collin, Robert E. Field Theory of Guided Waves. McGraw-Hill Book Company, Inc., New York, 1960.

4. Pennelegion, L. Advances in Hypervelocity Techniques. Plenum Press, 1962. (Proceedings of the Second Symposium on Hypervelocity Techniques, Denver, Colorado, March 1962).
5. Southworth, George C. Principles and Applications of Wave-Guide Transmission. D. Van Nostrand Company, Inc., New York, 1950.
6. Wylie, C. R., Jr. Advanced Engineering Mathematics. McGraw-Hill Book Company, Inc., New York, 1960. (Second Edition).

APPENDIX I  
WAVEGUIDE MODES

The mode in which a waveguide is excited determines the distribution of the electromagnetic fields in any plane perpendicular to the direction of propagation. When the electromagnetic equations are applied to circular guides, they are best written in cylindrical-coordinate form. The solutions to the electromagnetic equations in this form usually appear as Bessel functions. (This is in contrast with the case of rectangular guides, wherein the equations assume a rectangular-coordinate form, and their solutions appear as simple sinusoidal functions.)

The solutions to these electromagnetic equations can be divided into two basic sets of solutions representing two basic sets of propagation modes. For one set of modes, no axial magnetic field component exists. These modes have an axial component of electric field, however, and are called electric type (that is, E modes), or transverse magnetic (that is, TM modes). Modes in the other basic set have an axial magnetic field but no axial component of electric field and are, therefore, called magnetic type (that is, H modes), or transverse electric (that is, TE modes). The TM and TE designations are used in this appendix.

Of the many propagation configurations or modes of waves which may exist in circular guides, four rather well-known types are shown in Fig. 15, which has been adapted from Ref. 2. The dominant or lowest frequency mode in circular guides is the TE<sub>11</sub>, and it has found very general application. The TM<sub>01</sub> mode has found limited use in a few cases where circular symmetry is important, and the TE<sub>01</sub> mode has the advantage that for increasing frequency the attenuation in the guide decreases (Fig. 11 and Ref. 5). A further discussion of the Bessel function solutions previously mentioned is necessary to explain the subscripts which identify the various TE and TM modes.

The cutoff wavelength (i. e., the longest wavelength, referred to an unbounded medium, which can be propagated within the guide) and also the conditions for higher-order waves are related to the radius,  $b$ , of the guide by way of the zeroes of the particular Bessel function appropriate to the case in question. For example, the first of the configurations illustrated in Fig. 15 belongs to a family of waves which will be referred to as TM<sub>0n</sub>. They may be supported in a circular guide when:

$$2\pi a/\lambda \geq r_n, \quad \text{where } J'_0(r_n) = 0 \quad (1)$$

From tables of Bessel functions of zero order, it will be found that Eq. (1) may be satisfied when  $2\pi a/\lambda = 2.405, 5.52, 8.65$ , etc. These

values correspond respectively to values of the subscript,  $n$ , of 1, 2, 3, etc. (see Fig. 17).

The  $TM_{11}$  mode shown in Fig. 15 is the first in another family of waves referred to as  $TM_{1n}$ , and their respective cutoff wavelengths are specified by:

$$2\pi a/\lambda \geq r_n, \quad \text{where } J_1(r_n) = 0 \quad (2)$$

By referring to tables of Bessel functions of the first order, this equation is satisfied when  $2\pi a/\lambda = 3.83, 7.02, 10.17$ , etc. Again these values correspond to values of the subscript,  $n$ , of 1, 2, 3, etc. Other TM modes are possible in a circular guide when  $J_m(r_n) = 0$ , where  $m$  may assume any value from zero to infinity. Since each order  $m$  of the Bessel function may have any number of roots,  $n$ , we may expect a double infinity of roots. This complete family of modes is usually referred to as  $TM_{mn}$ .

The  $TE_{01}$  mode is the first in a series designated as  $TE_{0n}$ , and the relation to be satisfied is:

$$2\pi a/\lambda \geq r_n, \quad \text{where } J'_0(r_n) = 0 \quad (3)$$

In this case,  $J'_0(r_n)$  is the first derivative of  $J_0(r_n)$ . Values of  $J'_0(r_n)$  have been tabulated and appear in standard texts on Bessel functions. A well-known equality (Ref. 6) makes  $J'_0(r_n) = J_1(r_n)$ . Thus the cutoff wavelengths for  $TE_{0n}$  waves are the same as for  $TM_{1n}$  waves.

The first of a family of waves designated as  $TE_{1n}$  is the  $TE_{11}$  as shown in Fig. 15. The various modes of this family occur when:

$$2\pi a/\lambda \geq r_n, \quad \text{where } J'_1(r_n) = 0 \quad (4)$$

This may occur when  $2\pi a/\lambda = 1.84, 5.33, 8.54$ , etc. Other TE waves may occur when  $J'_m(r_n) = 0$ , where  $m$  may assume any value from zero to infinity. Since each order,  $m$ , of the Bessel function may have any number of roots from one to infinity, we may again expect a double infinity of waves, the  $TE_{mn}$  waves.

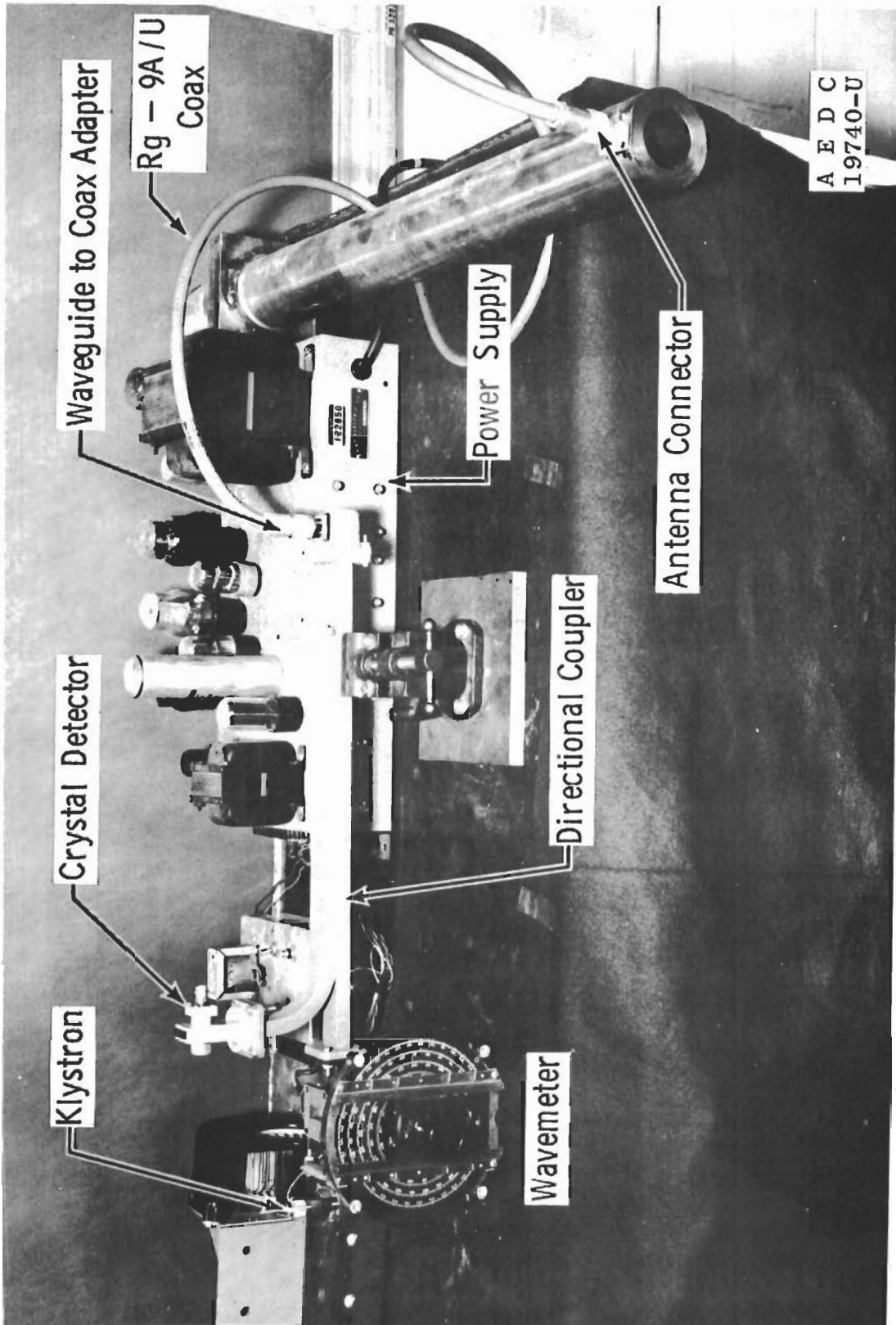


Fig. 1 Microwave Reflectometer Apparatus

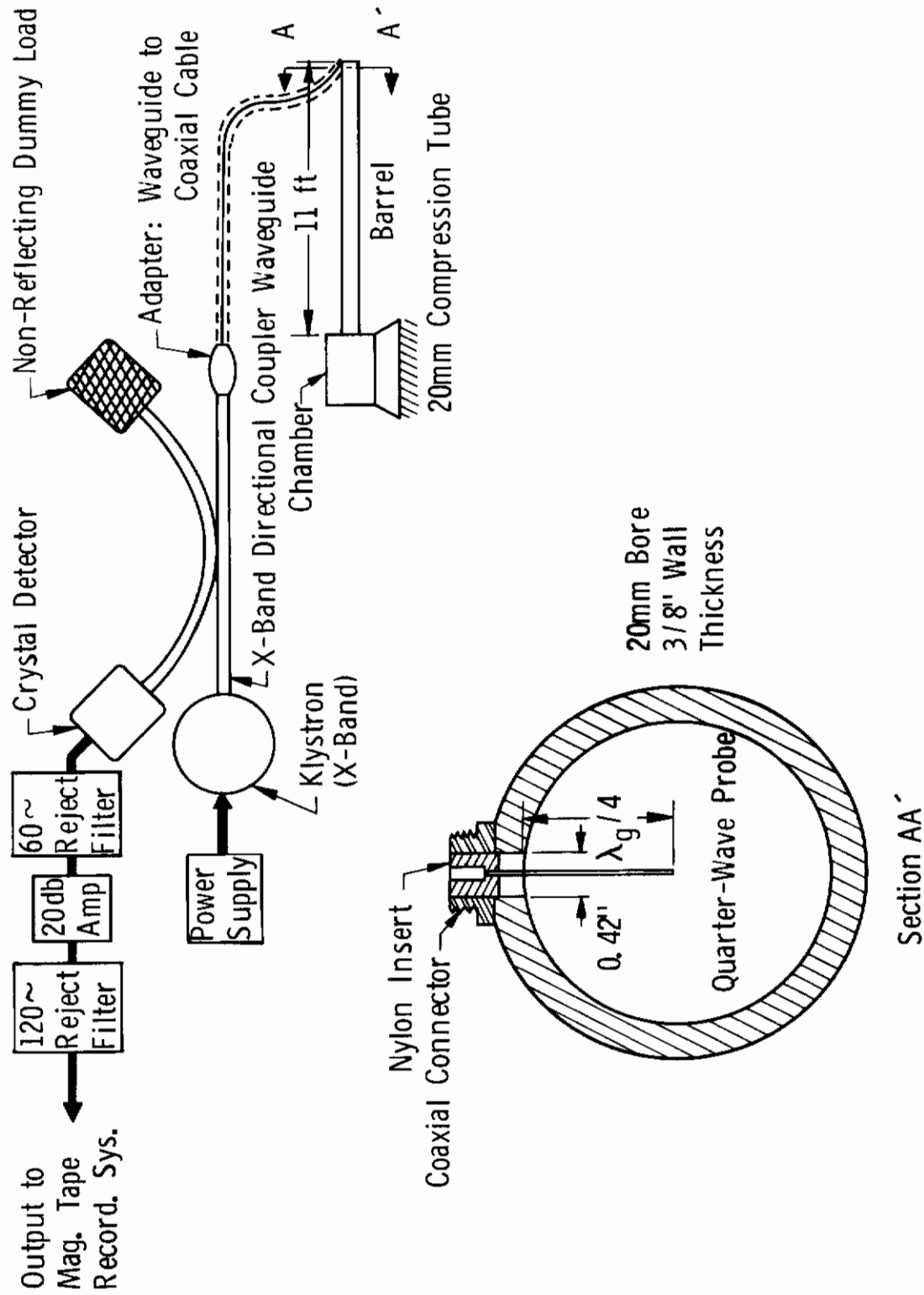


Fig. 2 Microwave Reflectometer with 20-mm Barrel

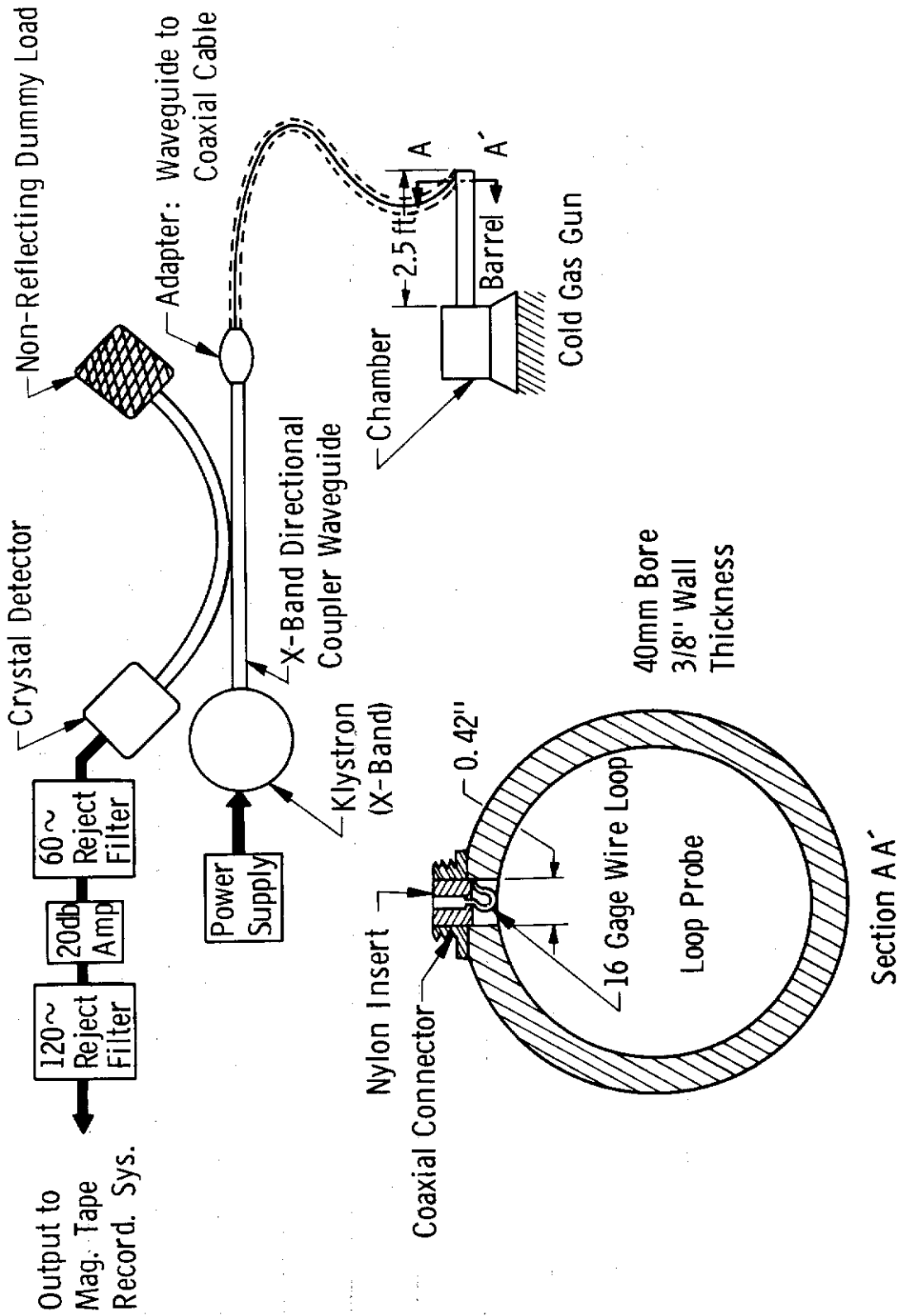


Fig. 3 Microwave Reflectometer with 40-mm Barrel

Order of Appearance	Mode	$r_n$	$\frac{\lambda_c}{b}$
1	TE <sub>11</sub>	1.841	3.413
2	TM <sub>01</sub>	2.405	2.613
3	TE <sub>21</sub>	3.054	2.057
4 and 5	TM <sub>11</sub>	3.832	1.640
4 and 5	TE <sub>01</sub>	3.832	1.640
6	TE <sub>31</sub>	4.201	1.496
7	TM <sub>21</sub>	5.136	1.223
8	TE <sub>41</sub>	5.318	1.181
9	TE <sub>12</sub>	5.331	1.179
10	TM <sub>02</sub>	5.520	1.138

$$\lambda_c = \frac{2\pi b}{r_n}$$

Where

$b$  = radius of waveguide

$r_n$  = zero solution of the proper Bessel function

Fig. 4 Cutoff Wavelengths for Circular Guides



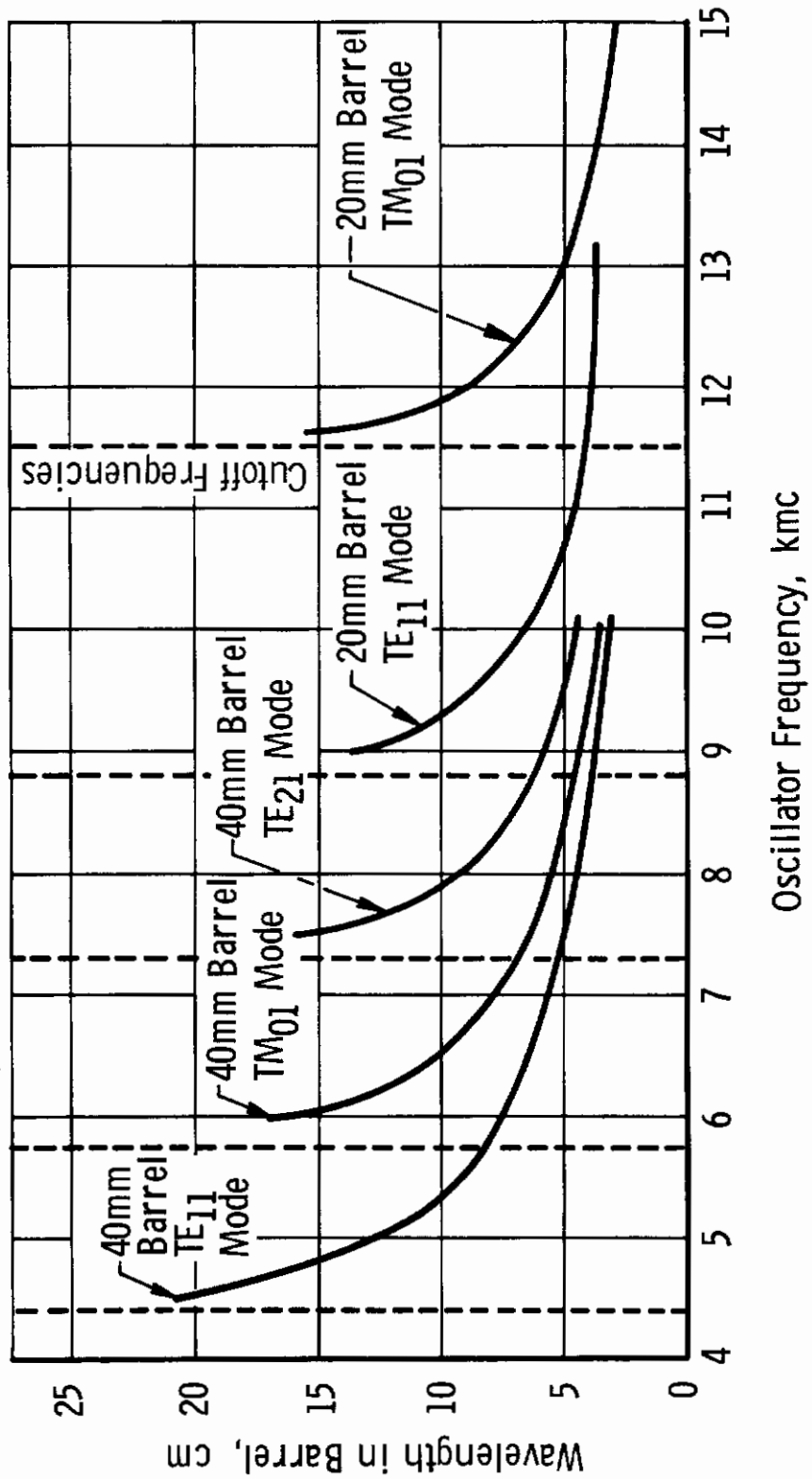


Fig. 5 Waveguide Wavelength versus Oscillator Frequency for Prevalent Modes in 20-mm and 40-mm Barrels

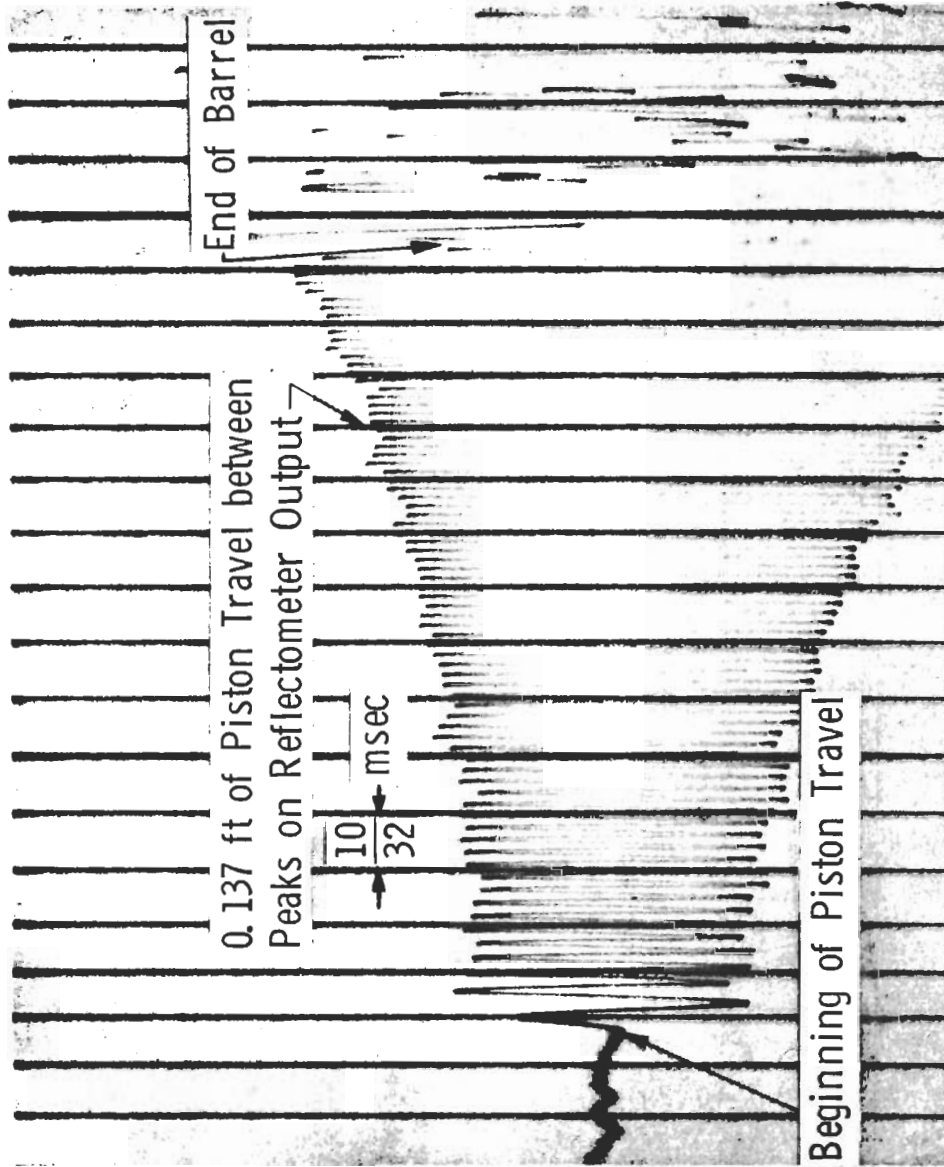


Fig. 6 Oscillogram: 20-mm Compression Tube Reflectometer Signal

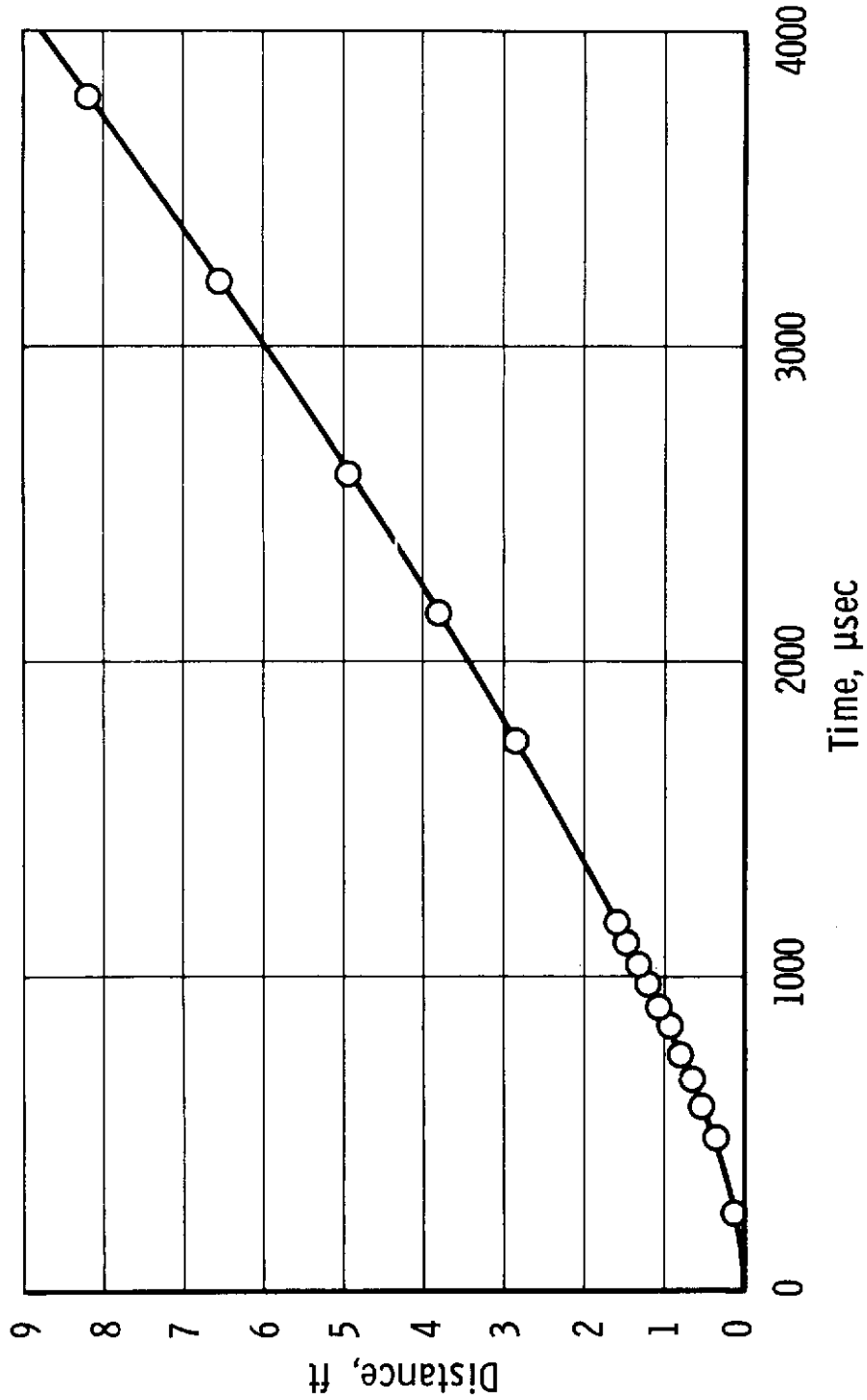


Fig. 7 20-mm Compression Tube Piston Displacement versus Time

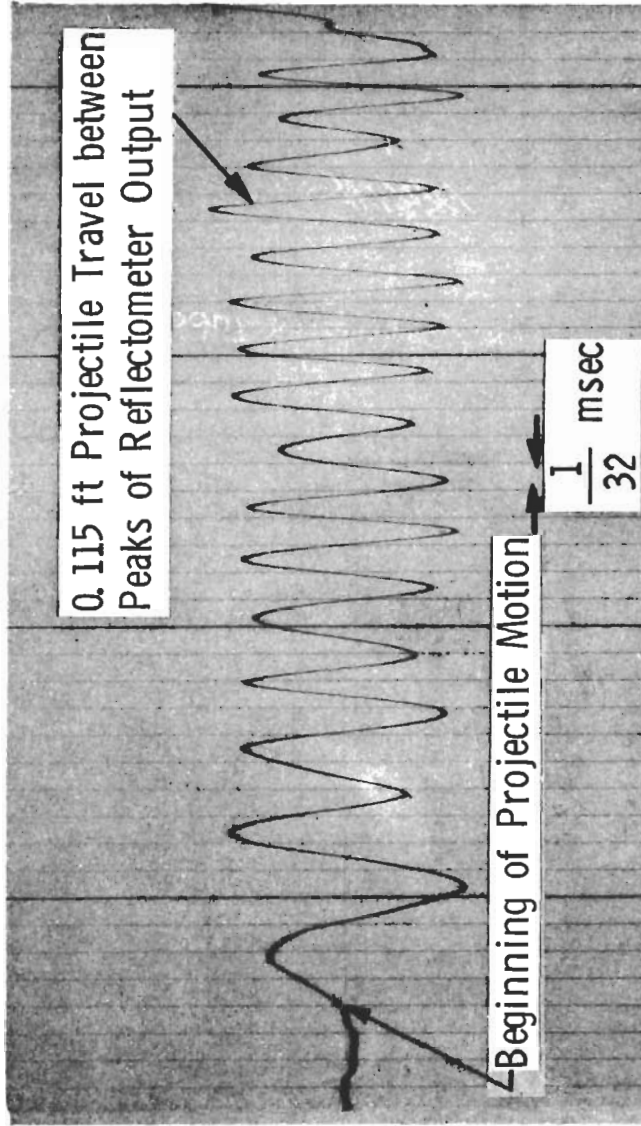


Fig. 8 Oscillogram: Medium Velocity, 40-mm Cold-Gas Gun Shot No. 401

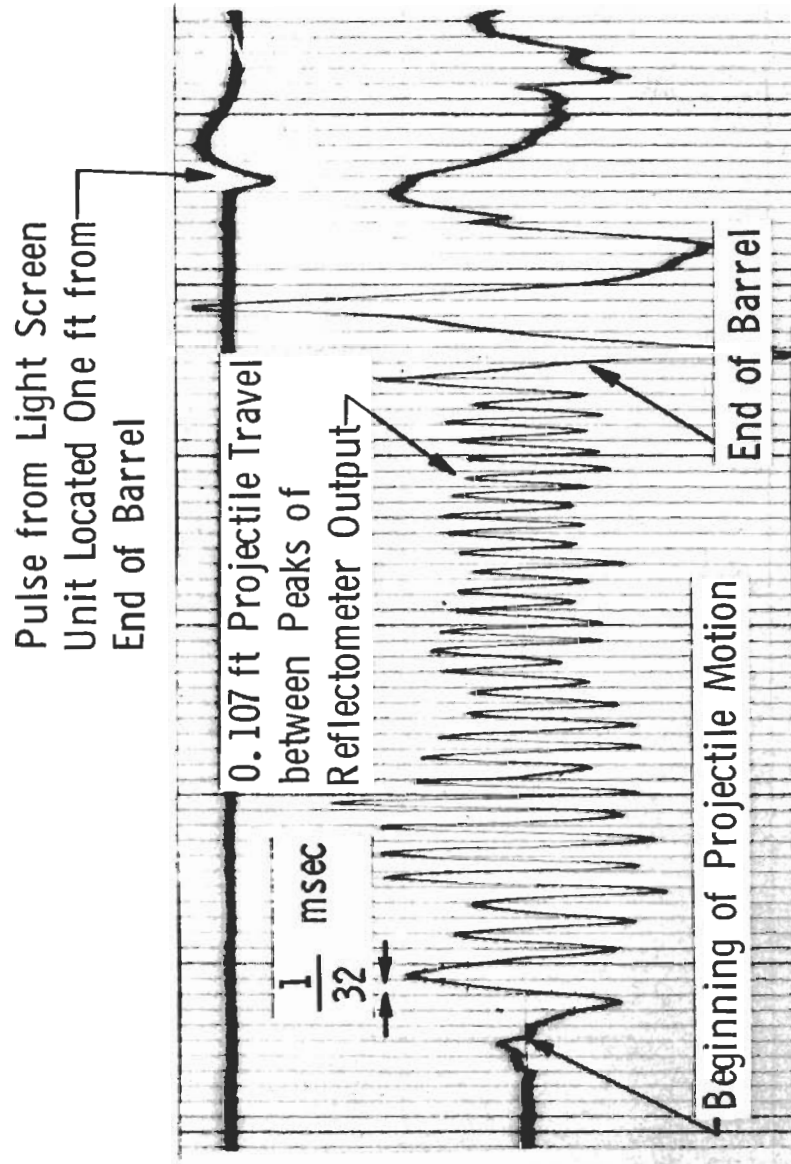


Fig. 9 Oscillogram: High Velocity, 40-mm Cold-Gas Gun Shot No. 466

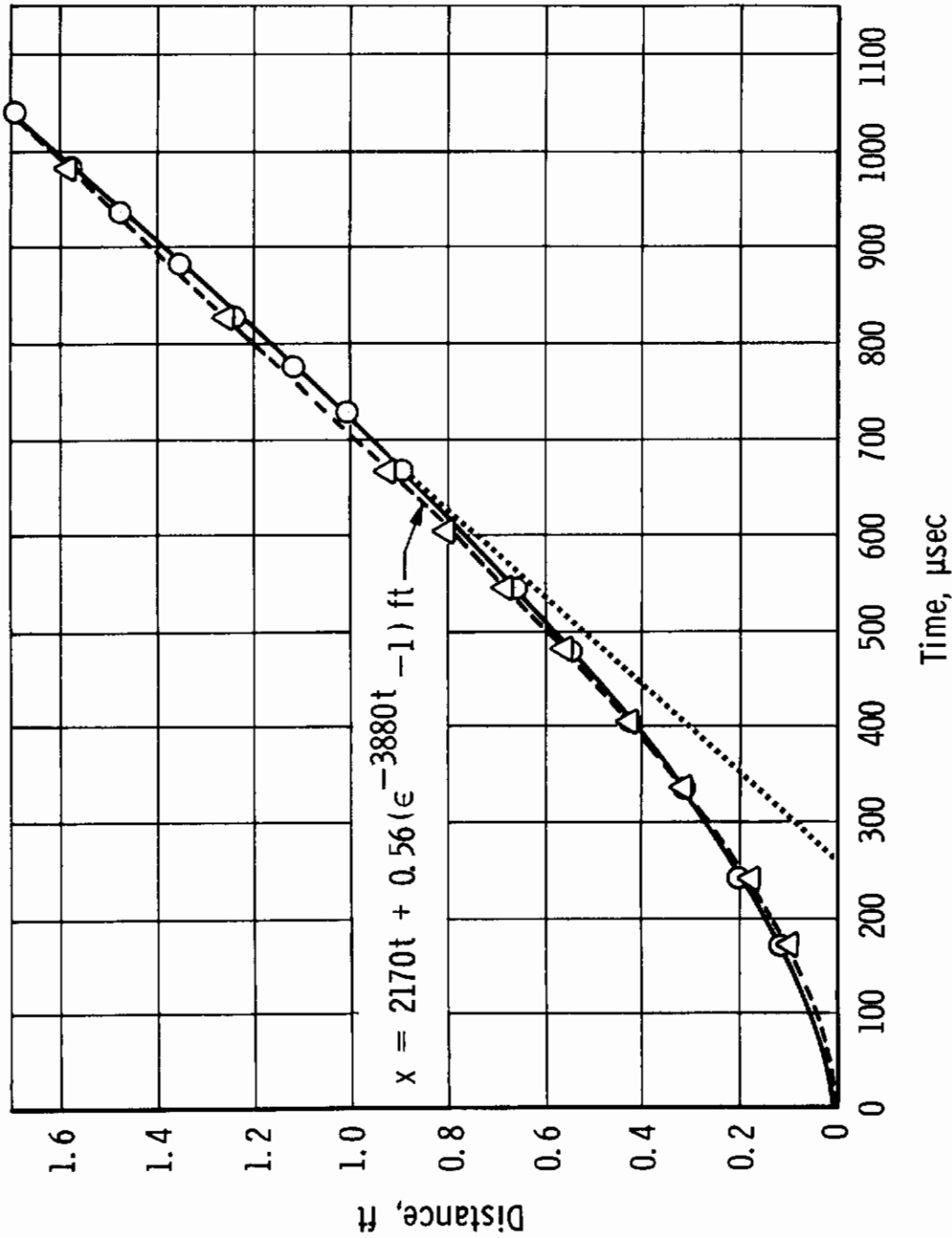


Fig. 10 40-mm Projectile Displacement versus Time, Shot No. 401

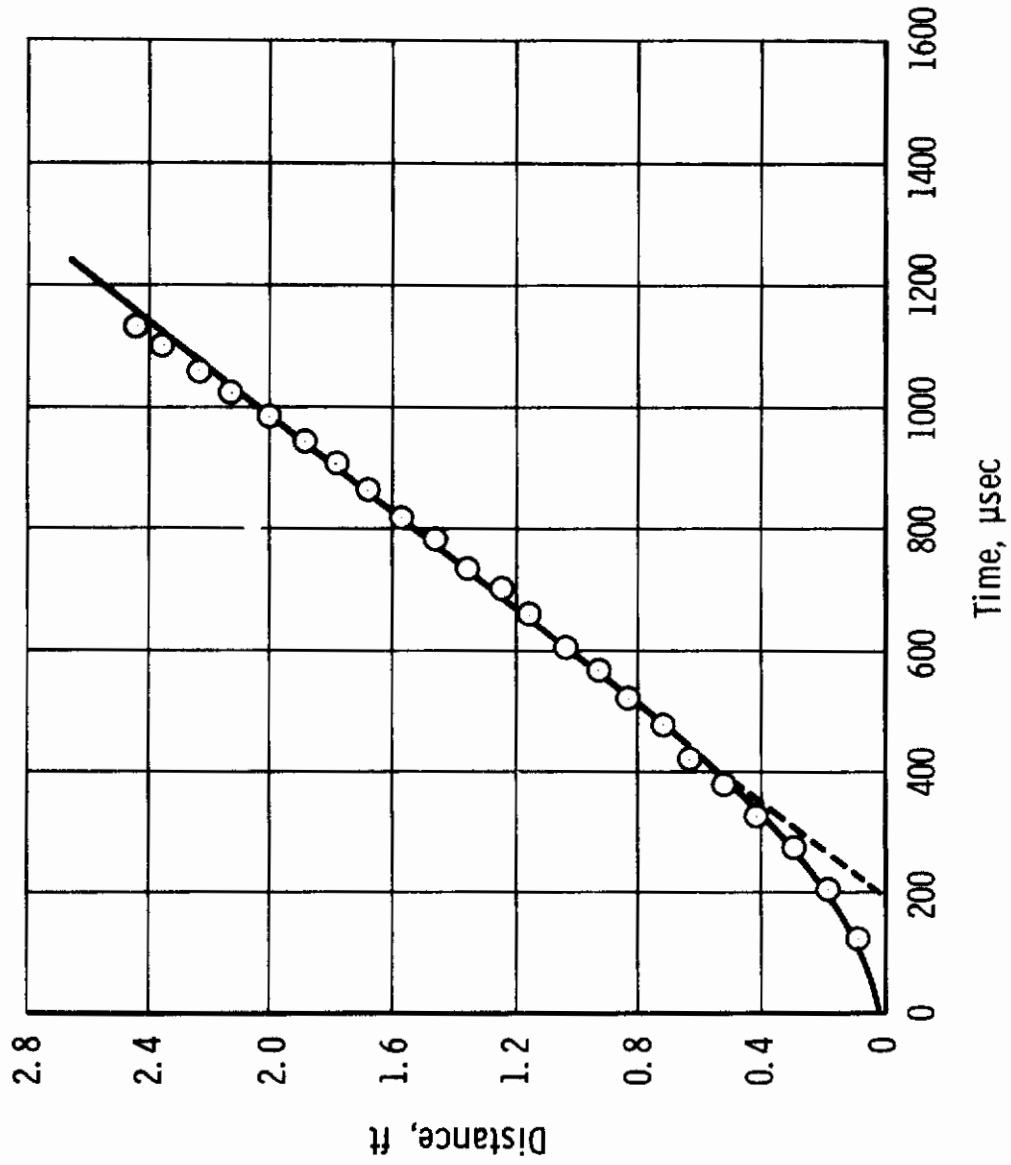


Fig. 11 40-mm Projectile Displacement versus Time, Shot No. 466

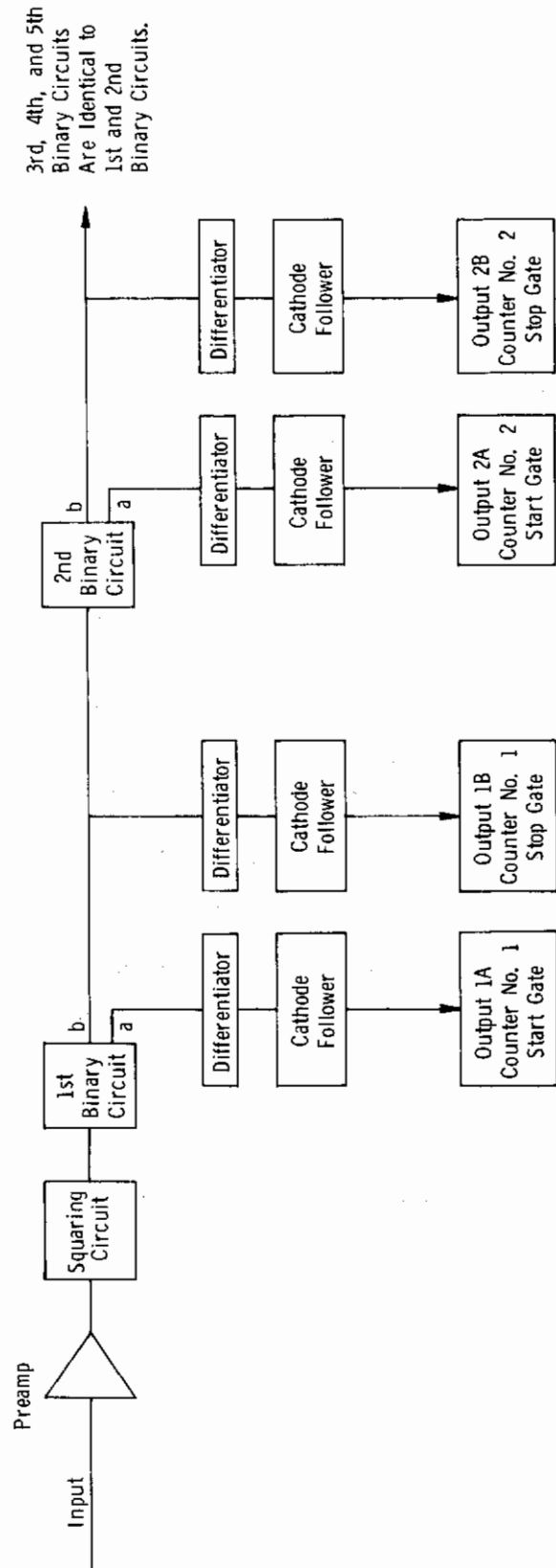


Fig. 1 2 Analog-to-Digital Reflectometer Readout System



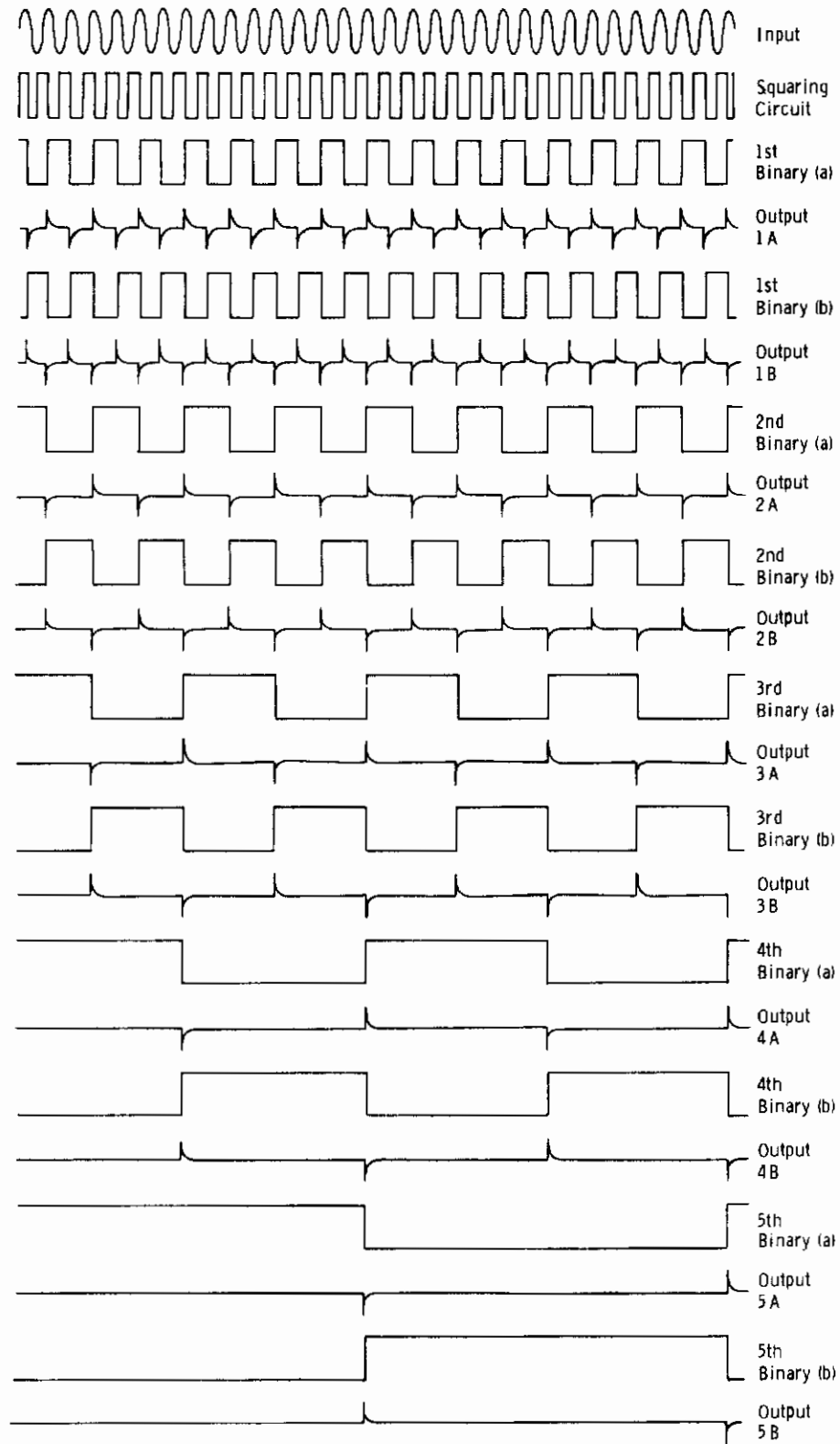


Fig. 13 Digital System Waveforms

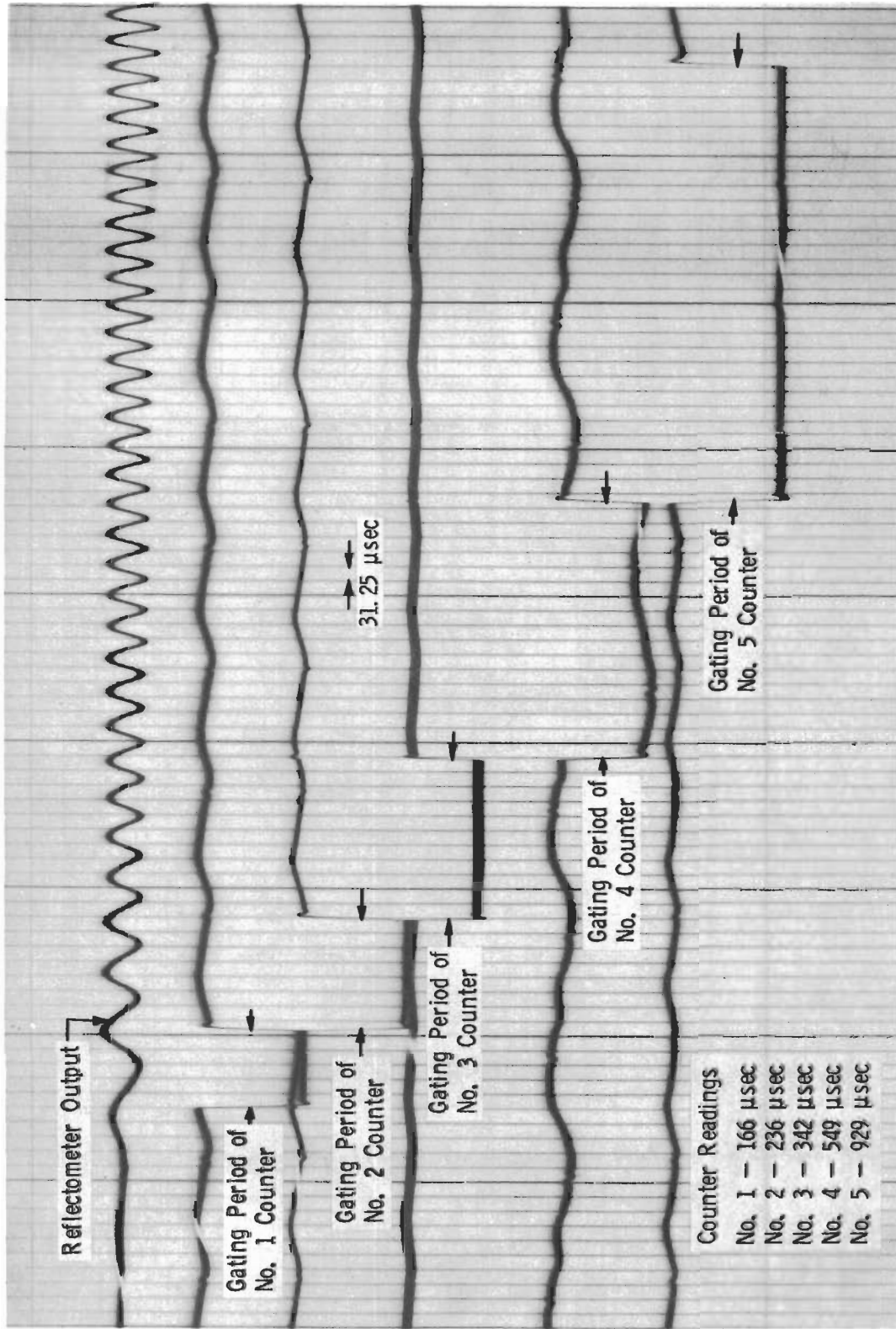


Fig. 14 Oscillogram: Digital System Operation

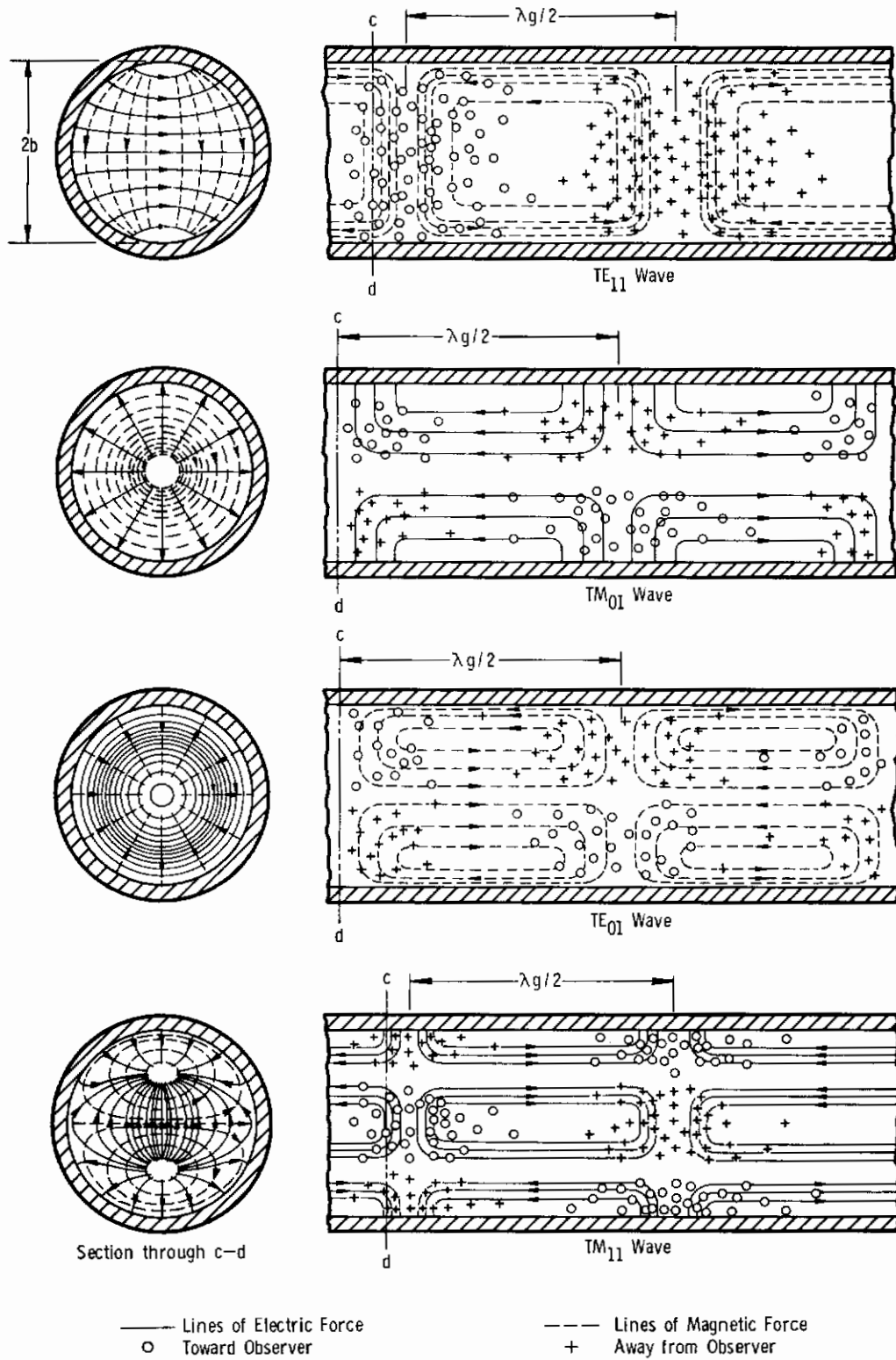


Fig. 15 Four of the Simple Modes of Waves in a Circular Waveguide

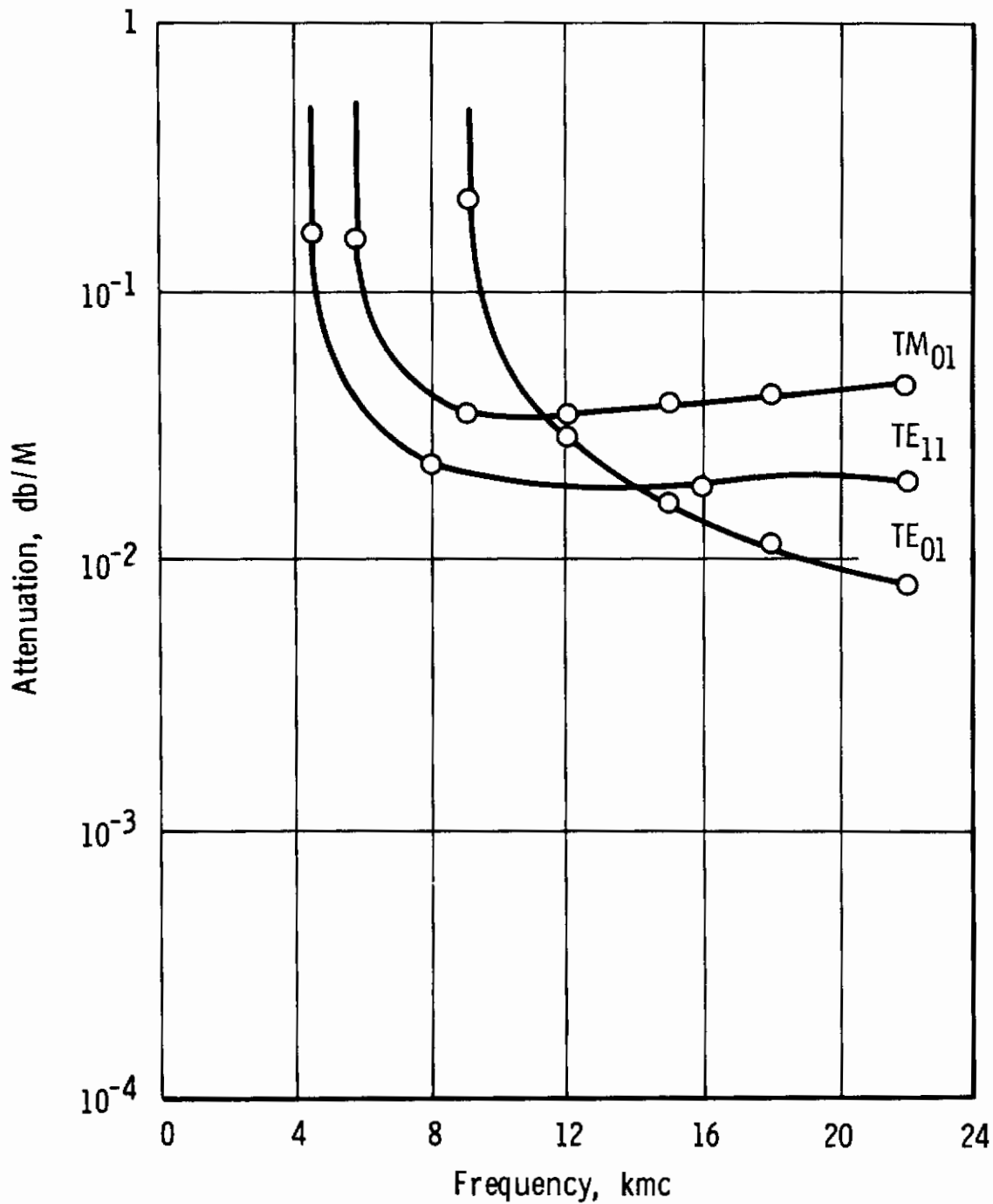


Fig. 16 Attenuation versus Frequency for a Hollow Copper Barrel with  $b = 20$  mm

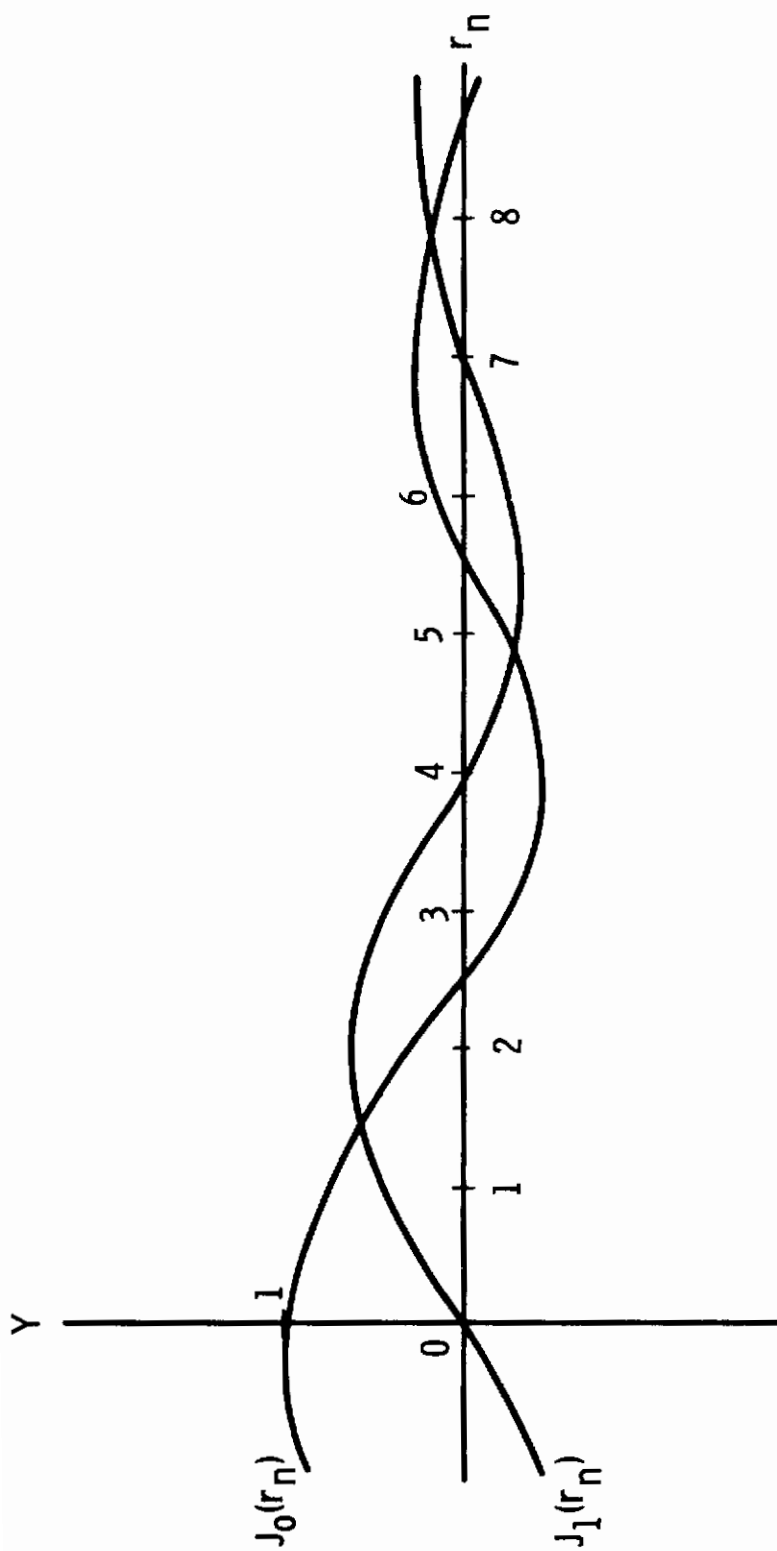


Fig. 17 Plot Showing the Bessel Functions of the First Kind,  $J_0(r_n)$  and  $J_1(r_n)$